Proceedings of the 2020 IEEE/SICE
International Symposium on System Integration
Honolulu, Hawaii, USA, January 12-15, 2020

Detecting Suspicious Objects With a Humanoid Robot Having a Metal Detector

Shunsuke Matsushima[1], Teppei Tsujita[1] and Satoko Abiko[2]

Abstract— **Security guard robots are required to patrol airports, warehouses, malls, etc. and to find and cope with the suspicious person. In this study, we aim to realize a patrol task by humanoid robots. An operator teleoperates a humanoid robot having a metal detector and swing the detector a short distance away from the surface of the suspect's clothing, and checks for hidden metal objects under the clothing. In order to develop this body scan system, the measurement range of the metal detector depending on the swing velocity was determined experimentally. Based on this knowledge, metal object detection experiment was conducted under 3 conditions: by human, by a teleoperated humanoid robot with/without a balance control. As a result, it was shown that the substitution of the body search work by the humanoid robot using the metal detector could not be sufficiently carried out only by the remote control of the simple right hand. Therefore, it is necessary to integrate the vision system for grasping the situation of the robot hand in the work and the whole body cooperation action and step action for the work range extension.**

I. INTRODUCTION

Robots are expected to do 3D, dull, dirty and dangerous, work instead of humans [1]. Security guard robots are a typical example. These are required to patrol airports, warehouses, malls, etc. and to find and cope with the suspicious person. It is a tedious and tiring task for humans to circle around these places. In addition, detecting and coping with a suspicious person is a dangerous task because it may be attacked by the suspicious person. Therefore, many security guard robots have been developed [2], [3], [4]. Due to the shortage of security guards, there is great expectation for these robots.

Recently, at Narita Airport in Japan, a security robot was introduced to secure the safety of Narita Airport, which is expected to have many users, in preparation for the Tokyo Olympics and Paralympics [5]. It is a wheel type robot of about 1.2 m in height, and it is equipped with a 360 ° camera and a metal detector. Unlike the gate type metal detector which is often seen in the airport, by mounting the metal detector on the mobile robot, it is possible to carry out the inspection as soon as the suspicious person or object is found during the patrol.

However, most of the above mentioned security robots are wheel type robots and can move only in the place where the environment for the robot is arranged. In this study, we aim to realize a patrol task by humanoid robots which can climb stairs [6] and walk on rough terrain [7] like a human. In this paper, we focused on body search with a handy metal detector, which is one of the patrol tasks. This makes it possible for robots to patrol places that can only be patrolled by human guards at present, such as large and complex athletic venues. We aim to achieve this task by teleoperating a humanoid robot having a metal detector. Body search is a task performed by a robot close to a person at close range, and it can be considered that a humanoid robot has an advantage that mental stress of a subject is smaller.

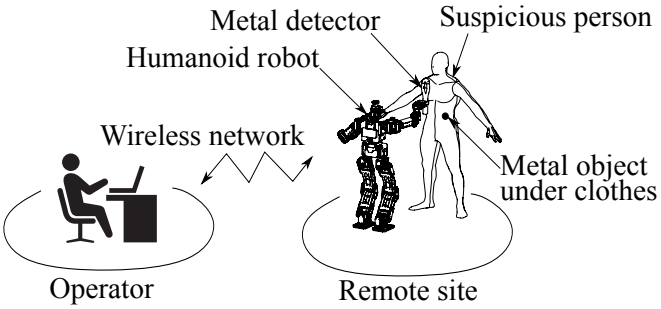

Fig. 1: An overview of body search with a teleoperated humanoid robot.

II. BODY SEARCH WITH A HUMANOID ROBOT

Fig. 1 shows an overview of a system to be realized in this study. As shown in this figure, an operator teleoperates a humanoid robot having a metal detector. The humanoid robot approaches the suspect, moves a metal detector a short distance away from the surface of the suspect's clothing, and checks for hidden metal objects under the clothing. In order to develop this body scan system, the following two items are required to be discuss.

1) How far should a metal detector move from the surface of the clothing and how fast should it move?
2) How to move a metal detector while maintaining balance of a humanoid robot?

The above mentioned items 1) and 2) are discussed in Section III and Section IV, respectively. In addition, a developed body search system is evaluated in Section V. Section VI summarizes conclusions.

III. CHARACTERISTICS OF A METAL DETECTOR

A. Metal Detector

In this research, handy metal detector GC-101H (Doradus Corp.) is used to detect suspicious objects. Metal detectors

[1]Shunsuke Matsushima and Teppei Tsujita are with Department of Mechanical Engineering, National Defense Academy of Japan, 1-10-20 Hashirimizu, Yokosuka, Kanagawa, 239-8686, Japan. em58051@nda.ac.jp, t.tsujita@ieee.org

[2]Satoko Abiko is with Department of Electrical Engineering, Shibaura Institute of Technology, 3-7-5, Toyosu, Koto-ku, Tokyo, 135-8548, Japan abiko@shibaura-it.ac.jp

978-1-7281-6667-4/20/$31.00 ©2020 IEEE

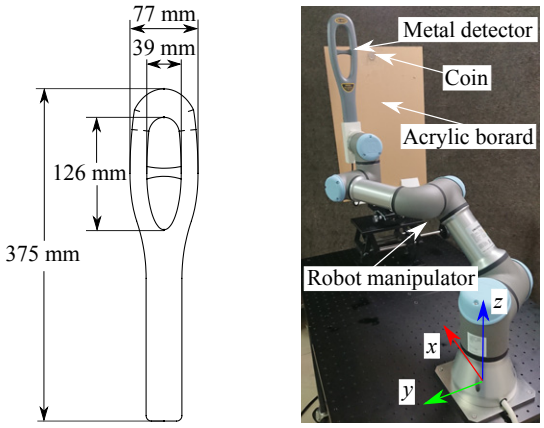

(a) Dimensions of the detector (b) An overview

Fig. 2: Experimental setup for determining the measurement range.

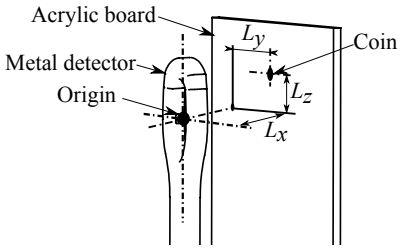

Fig. 3: Definitions of the measurement range.

can detect knives, handguns, and fuses for bombs, etc. The weight of the detector is 190 g (not including battery) and it can be operated with one hand, and its dimensions are as shown in Fig. 2 (a). The measurement range of this metal detector was experimentally determined. The sensitivity of this metal detector can be adjusted by a variable resistance and this device can notify by sound when metal is detected.

B. Experimental Setup

In this paper, a 100 japanese yen coin which is made of 75% copper and 25% nickel is used as a metal object to be detected. The diameter and weight of the coin are 22.6 mm and 4.8 g, respectively. In order to measure the maximum detection distance of the metal detector, the detector was attached to the end effector of robot manipulator UR3 (Universal Robots A/S) as shown in Fig. 2 (b). The metal detector was moved parallel by the manipulator to the acrylic plate to which the coin is attached at distance L_x. Fig. 3 shows the definitions of the measurement range. The detecter was moved horizontally from $L_y = -100$ mm to 100 mm from the center of the coin at the velocity v_y, and the relationship between the minimum velocity required for detecting a coin and the distance L_x was observed.

In this experiment, the metal detector was moved left and right five times. Thus, the detector passed over the coin 10 times. Since the operating manual of the metal detector stated that metal cannot be detected in the fixed state, the device was moved at $v_y = 10$ mm/s or more ($v_y \leq 200$ mm/s). The velocity in the case that the alarm sounded more than eight

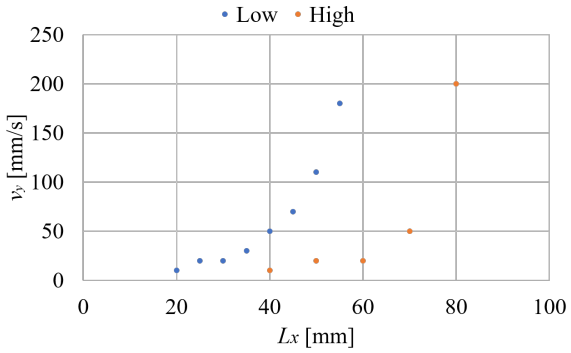

Fig. 4: Relationship between distance L_x and horizontal velocity v_y ($L_z = 0$ mm).

times when it passed over the coin was determined as the minimum velocity. This minimum velocity was determined in increments of 10 mm/s while varying the moving velocity.

C. Experimental Results

Fig. 4 shows the relationship between distance L_x and horizontal velocity v_y when $L_z = 0$ mm. The orange dots or the blue dots indicate the minimum required velocities when the sensitivity of the sensor is high or low, respectively. This figure shows that, as the distance from the coin increases, the required moving speed increases exponentially. The conceivable reason is as follows. The primary coil in the metal detector produces an alternating magnetic field, and if there is an object made of electrically conductive metal in the primary magnetic field, an eddy current is induced in the object. This eddy current also produces a magnetic field of its own and the secondary coil in the device detects the change in the magnetic field due to the eddy current. The induced electromotive force V in the secondary coil is given by:

$$V = -n \cdot \frac{\delta \Phi}{\delta t}, \tag{1}$$

where n, Φ and t are a number of turns, the magnetic flux passing through a coil and time, respectively [8]. The flux density change denoted in the right side of Eq. (1) is caused not only by the alternating magnetic field produced by the primary coil but also by the motion of the secondary coil. Therefore, even if the distance to the coin increases, it can be detected by increasing the moving speed.

Fig. 4 shows that the sensitivity affects the sensing distance and the coin can be detected by moving over 50 mm/s even at a distance of L_x= 70 mm when the sensitivity is high. The sensing range of the detector in z axis direction is $\pm$ 63 mm from its origin according to its operating manual. This relationship will be used to verify the search range of the experiment in Chapter V.

IV. Teleoperation System for Swinging a Metal Detector

Fig. 5 shows an overview of the developed teleoperation system for swinging the metal detector. Life-sized humanoid

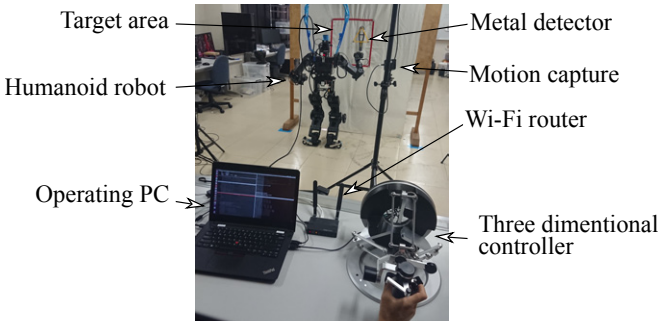

Fig. 5: An overview of the developed teleoperation system for swinging the metal detector.

robot THORMANG3 (ROBOTIS Co.) [9] grasps the metal detector with its right hand and swings the metal detector without changing the position of both soles. THORMANG3 is the successor to THORMANG used in DARPA Robotics Challenge [10]. This humanoid robot has two legs with six DoFs (Degrees of Freedom), two arms with seven DoFs and one DoF gripper, a neck with two DoFs and a waist with one DoF. Therefore, the total DoF (without the grippers) of THORMANG3 is 29. Its height and weight are 1375 mm and 42 kg, respectively. Fig. 6 shows a system diagram of the developed teleoperation system. Three dimensional controller Omega.7 (Force dimensions) [11] is used for the master controller of this teleoperation system. This controller sends reference velocity of the right hand of the humanoid robot. Fig. 7 shows notations used in the following subsections. Σ_0 and Σ_B are the inertial coordinate system and the coordinate system fixed in the base link, respectively.

A. Master system

Omega.7 can measure the six DoFs position/orientation of its end-effector and the state of the gripper. Although Omega.7 can display translational forces, the reference display forces are set to be zero in this preliminary system. In the master system, Omega.7 is connected to a computer running Ubuntu linux 16.04 LTS via USB (Universal Serial Bus) and sends current position $\boldsymbol{p}_t \in \Re^{3\times1}$ to programs working on ROS (Robot Operating System) [12].

The translational movable range Omega.7 is very small compared to the movable range of the end effector of the humanoid robot. Therefore, the reference translational velocity of the end-effector of the right arm of the humanoid robot $\boldsymbol{v} \in \Re^{3\times1}$ in Σ_0 coordinate system is computed as follows:

$$\boldsymbol{v}^{ref} = K_v(\boldsymbol{p}_t - \boldsymbol{p}_0), \tag{2}$$

where K_v and $\boldsymbol{p}_0 \in \Re^{3\times1}$ a gain of the velocity controller and the position of the end-effector when the operator grasped the gripper of the interface, respectively. On the other hand, the reference angular velocity of the end-effector $\boldsymbol{\omega}^{ref} \in \Re^{3\times1}$ in Σ_0 coordinate system is given as follows:

$$\boldsymbol{\omega}^{ref} = \boldsymbol{0}. \tag{3}$$

When the the operator does not grasp the gripper, $\boldsymbol{v}^{ref}$ is set to be zero. These reference velocities are sent to the slave system by ROS topics every 8 ms via WiFi network.

B. Slave system

In the slave system, the reference velocities are received by a control computer mounted on the humanoid robot. Programs working on this computer sends reference joint angles to joint modules. The reference joint angles are computed to satisfy the reference velocity of the end-effector while maintaining balance of the humanoid robot based on the resolved momentum control method [13]. In order to obtain all reference joint angles, references of the linear momentum, the angular momentum, the sole velocities and the hand velocity in Σ_0 coordinate system are specified.

1) Reference momentums and velocities: In order to keep its balance, the reference linear momentum $\boldsymbol{P}^{ref} \in \Re^{3\times1}$ is given to maintain the initial centroid position as follows:

$$\boldsymbol{P}^{ref} = \tilde{m}K_P(\tilde{\boldsymbol{c}}^{ref} - \tilde{\boldsymbol{c}}), \tag{4}$$

where $\tilde{m}$, $\tilde{\boldsymbol{c}} \in \Re^{3\times1}$ and $\tilde{\boldsymbol{c}}^{ref} \in \Re^{3\times1}$ are the total mass of the robot, the total center of mass (CoM) and the reference total CoM, respectively. By Eq. (4), the total CoM is always controlled to be the reference CoM even if disturbance is applied. The reference angular momentum $\boldsymbol{L}^{ref} \in \Re^{3\times1}$ around CoM is given as follows:

$$\boldsymbol{L}^{ref} = \boldsymbol{0}. \tag{5}$$

The reference velocity vector of the end-effector of the right arm (Arm 3) $\boldsymbol{\xi}_3^{ref} \in \Re^{6\times1}$ is denoted as follows from Eqs. (2) and (3):

$$\boldsymbol{\xi}_3^{ref} = \begin{bmatrix} \boldsymbol{v}^{ref\,T} & \boldsymbol{\omega}^{ref\,T} \end{bmatrix}^T. \tag{6}$$

In this case, the robot does not change its standing position. Therefore, the reference velocities of the soles $\boldsymbol{\xi}_i^{ref} \in \Re^{6\times1}$ are zero as follows:

$$\boldsymbol{\xi}_i^{ref} = \boldsymbol{0} \qquad (i = 1 \text{ or } 2). \tag{7}$$

2) Resolved momentam control [13]: From the reference values given by Eqs. (4)–(7), all reference velocities of the joints are obtained. The velocities of end-effectors of Arm $1 \sim 3$ shown in Fig. 7 are given, and joints of the neck and the waist are fixed. The angular velocity vector of joints surrounded by a dotted line named "Arm 4" in Fig. 7 $\dot{\boldsymbol{\theta}}_4 \in \Re^{7\times1}$ and $\boldsymbol{\xi}_B \equiv \begin{bmatrix} \boldsymbol{v}_B{}^T & \boldsymbol{\omega}_B{}^T \end{bmatrix}^T$, where $\boldsymbol{v}_B \in \Re^{3\times1}$ and $\boldsymbol{\omega}_B \in \Re^{3\times1}$ are the linear velocity vector and the angular velocity vector of the origin of Σ_B coordinate system in Σ_0 coordinate system, respectively, can be obtained as follows:

$$\begin{bmatrix} \boldsymbol{\xi}_B \\ \dot{\boldsymbol{\theta}}_4 \end{bmatrix} = \boldsymbol{A}^{\dagger}\boldsymbol{y}, \tag{8}$$

where $*^{\dagger}$ represents the pseudo-inverse matrix of matrix $*$. $\boldsymbol{A} \in \Re^{6\times13}$ and $\boldsymbol{y} \in \Re^{6\times1}$ are defined as follows:

$$\boldsymbol{A} \equiv \begin{bmatrix} \boldsymbol{M}_B^* & \boldsymbol{M}_4 \\ \boldsymbol{H}_B^* & \boldsymbol{H}_4 \end{bmatrix}, \tag{9}$$

$$\boldsymbol{y} \equiv \begin{bmatrix} \boldsymbol{P}^{ref} \\ \boldsymbol{L}^{ref} \end{bmatrix} - \sum_{i=1}^{3} \begin{bmatrix} \boldsymbol{M}_i^* \\ \boldsymbol{H}_i^* \end{bmatrix} \boldsymbol{\xi}_i^{ref}, \tag{10}$$

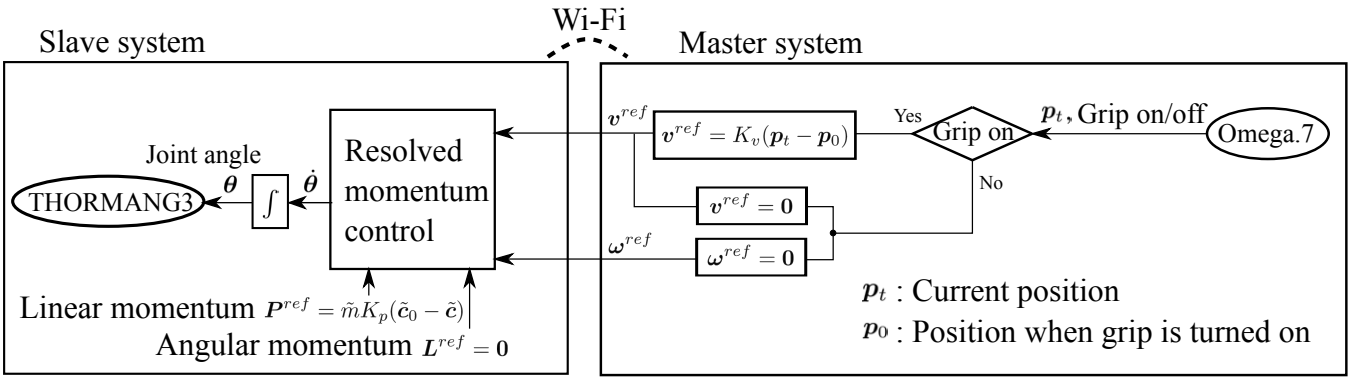

Fig. 6: System diagram of the teleoperation system.

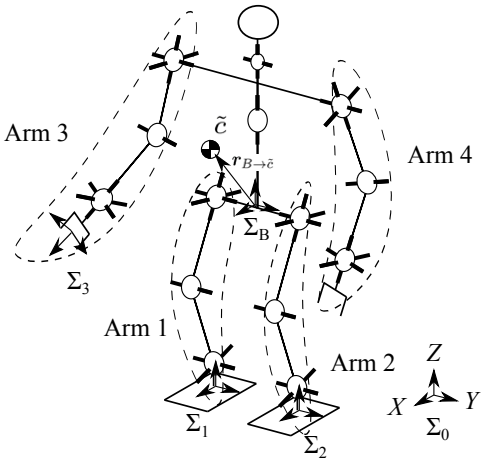

Fig. 7: Notations for the humanoid robot.

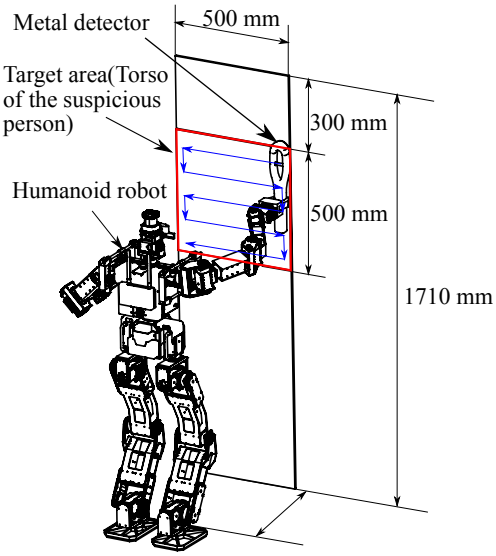

Fig. 8: Experiment of body scanning task with a humanoid robot.

where $\boldsymbol{M}_4 \in \Re^{3\times7}$ and $\boldsymbol{H}_4 \in \Re^{3\times7}$ are inertial matrices corresponding to $\dot{\boldsymbol{\theta}}_4$. $\boldsymbol{P}^{ref}$ given by Eq. (4), $\boldsymbol{L}^{ref}$ given by Eq. (5) and $\boldsymbol{\xi}_i^{ref}$ given by Eqs. (7) and (6) are substituted into Eq. (10). Here, $\boldsymbol{M}_B^* \in \Re^{3\times3}$, $\boldsymbol{H}_B^* \in \Re^{3\times3}$, $\boldsymbol{M}_i^* \in \Re^{3\times3}$ and $\boldsymbol{H}_i^* \in \Re^{3\times3}$ are denoted as follows:

$$\begin{bmatrix}\boldsymbol{M}_B^* \\ \boldsymbol{H}_B^*\end{bmatrix} \equiv \begin{bmatrix}\tilde{m}\boldsymbol{E} & -\tilde{m}\hat{\boldsymbol{r}}_{B\to c} \\ \boldsymbol{0} & \tilde{\boldsymbol{I}}\end{bmatrix} - \sum_{i=1}^{3}\begin{bmatrix}\boldsymbol{M}_i^* \\ \boldsymbol{H}_i^*\end{bmatrix}\begin{bmatrix}\boldsymbol{E} & -\hat{\boldsymbol{r}}_{B\to i} \\ \boldsymbol{0} & \boldsymbol{E}\end{bmatrix},$$

$$\begin{bmatrix}\boldsymbol{M}_i^* \\ \boldsymbol{H}_i^*\end{bmatrix} \equiv \begin{cases}\begin{bmatrix}\boldsymbol{M}_i \\ \boldsymbol{H}_i\end{bmatrix}\boldsymbol{J}_i^{-1} & (i = 1 \text{ or } 2) \\ \begin{bmatrix}\boldsymbol{M}_i \\ \boldsymbol{H}_i\end{bmatrix}\boldsymbol{J}_i^{\dagger} & (i = 3)\end{cases},$$

where $\boldsymbol{E} \in \Re^{3\times3}$ and $\hat{\boldsymbol{I}} \in \Re^{3\times3}$ are an identity matrix and the total inertia matrix with respect to the CoM, respectively. $\boldsymbol{r}_{B\to c} \in \Re^{3\times1}$ is a vector from the origin of Σ_B to the CoM, $\boldsymbol{r}_{B\to i} \in \Re^{3\times1}$ is a vector from the origin of Σ_B to the end-effector of i-th arm, and $\hat{*}$ is an operator which translates a vector $* \in \Re^{3\times1}$ into a skew symmetric matrix. $\boldsymbol{M}_i \in \Re^{3\times n_i}$, $\boldsymbol{H}_i \in \Re^{3\times n_i}$ and $\boldsymbol{J}_i \in \Re^{6\times n_i}$ are the inertial matrix for the linear momentum of the i-th arm the inertial matrix for the angular momentum of the i-th arm and the Jacobian matrix of the i-th arm, respectively. n_i is the number of DoFs of the i-th arm.

By using $\boldsymbol{\xi}_B$ obtained by Eq. (8), joint velocity vector of i-th arm $\boldsymbol{\theta}_i$ can be obtained as follows:

$$\dot{\boldsymbol{\theta}}_i = \begin{cases} -\boldsymbol{J}_i^{-1}\begin{bmatrix}\boldsymbol{E} & -\hat{\boldsymbol{r}}_{B\to i} \\ \boldsymbol{0} & \boldsymbol{E}\end{bmatrix}\boldsymbol{\xi}_B & (i = 1 \text{ or } 2) \\ \boldsymbol{J}_i^{\dagger}\left\{\boldsymbol{\xi}_i^{ref} - \begin{bmatrix}\boldsymbol{E} & -\hat{\boldsymbol{r}}_{B\to i} \\ \boldsymbol{0} & \boldsymbol{E}\end{bmatrix}\right\} & (i = 3)\end{cases}.$$

By integrating joint velocities $\dot{\boldsymbol{\theta}}_i$ (i =1∼4) numerically, all joint angles can be obtained and are sent to smart actuators in the humanoid robot.

V. Experiment

In this experiment, the target area of the metal detection was set at 500 mm × 500 mm square on the assumption of the torso of the Japanese man of about 171 cm in average height. On the assumption that the length from the head to the neck is 300 mm, the upper half of the body, excluding the head to the neck, was regarded as the target area of the scan, and the experimental conditions were set as shown in the Fig. 8. With the aim of tracing the entire area of 500 mm × 500 mm, experiments were conducted 3 times each under 3 conditions: by human, by teleoperated humanoid robot with the resolved momentum control, and by the teleoperated

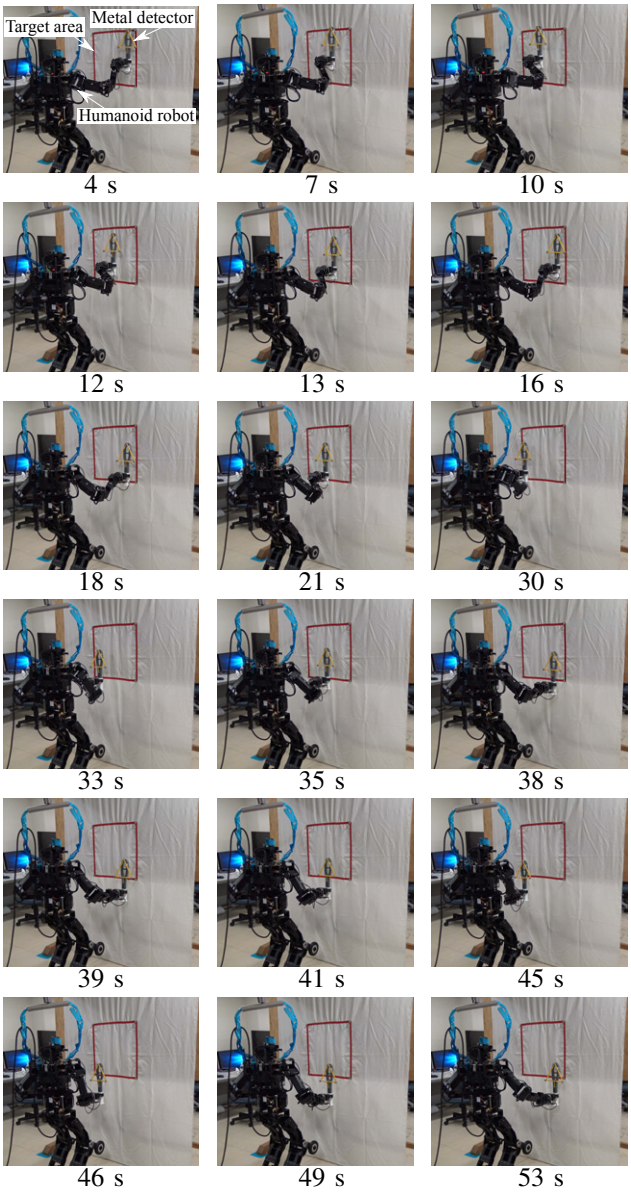

Fig. 9: Metal detecting task experiment with teleoperated humanoid robot.

humanoid robot without the resolved momentum control (the right arm is only controlled by the master controller). Fig. 10 (a) shows the path and scanned area by human. The blue line is the end-effector's path when L_x is in detection range, the gray line is the end effector position when L_x is out of detection range, and the green line shows the metal detector's sensing range in z axis direction described in III-C. The scanning time was about 12 seconds on average. As can be seen from Fig. 10 (a), all path are in proper working distance.

Next, Fig. 10 (b) shows the hand position controlled by the teleoperation system with the resolved momentum control. Fig. 9 shows snapshots. It took approximately 45 second to operate the robot. The resolved momentum control need some parameter, K_v and K_P and $\tilde{c}^{ref}$, and these parameters were determined heuristically. In this study, K_v is 2 1/s, K_P is 5 1/s, and $\tilde{c}^{ref}$ is CoM position when executed the program of resolved momentum control. As can be seen from Fig. 10 (b), there are many gray points that cannot be measured due to out of range or lack of speed. The reason for this is that the operator does not know the distance between its hand and the target plane, and is not able to get the detector close to the target plane. And, it is also considered that the sufficient speed has not been produced with it. In addition, comparing with Fig. 10 (a), the measurement range in the y axis direction and the z axis direction is narrower as a whole. This is because the arm was stretched out during the operation, and it became out of the operable range. In particular, it can be seen that the upper left of the target area is not measured. This is because the wrist joint has reached the joint angle limit. In the resolved momentum control, the target value of the linear momentum is set so that the center of mass position does not change. When the hand moves are moved to the left, the body moves to the right to maintain the center of mass. As a result, the posture becomes severe because the arm must be relatively extended to the left, and the joint angles reach their limit.

Fig. 10 (c) shows the hand position obtained by teleoperated the humanoid robot using inverse kinematics with only right arm (Seven DoFs) without resolved momentum control. It took approximately 59 second to operate the robot. In the motion by the inverse kinematics of the right arm, the stability of the balance is not guaranteed since the center of mass is not controlled like resolved momentum control, but it was shown that the workspace was not narrowed and it could cover the wider area than the resolved momentum control.

From this experiment, it was shown that the substitution of the body search work by the humanoid robot using the metal detector could not be sufficiently carried out only by the remote control of the simple right hand. And, it is necessary to control the whole body by moving the center of mass in order to ensure the working space. However, since humanoid robots are floating based, they can be solved by taking a strategy of stepping before getting into such a severe posture. And, it was shown that the operation time by the robot was about 5 times longer than that by the human, and that even within the moveable range of the end effector, a metal object may not be measured because the position of the sensor is outside the measurement range of the sensor. This is thought to be because it is difficult to understand the distance between the end effector and the object by the remote control. Although all experiments using the humanoid robot were conducted by a well-trained operator, the coverage area is not sufficient. Therefore, it is necessary to integrate the vision system for grasping the situation of the robot hand in the work and the whole body cooperation action and step action for the work range extension.

VI. CONCLUSIONS

In this paper, in order to perform body search tasks using the metal detector by a humanoid robot, the measurement range of the metal detector was determined experimentally.

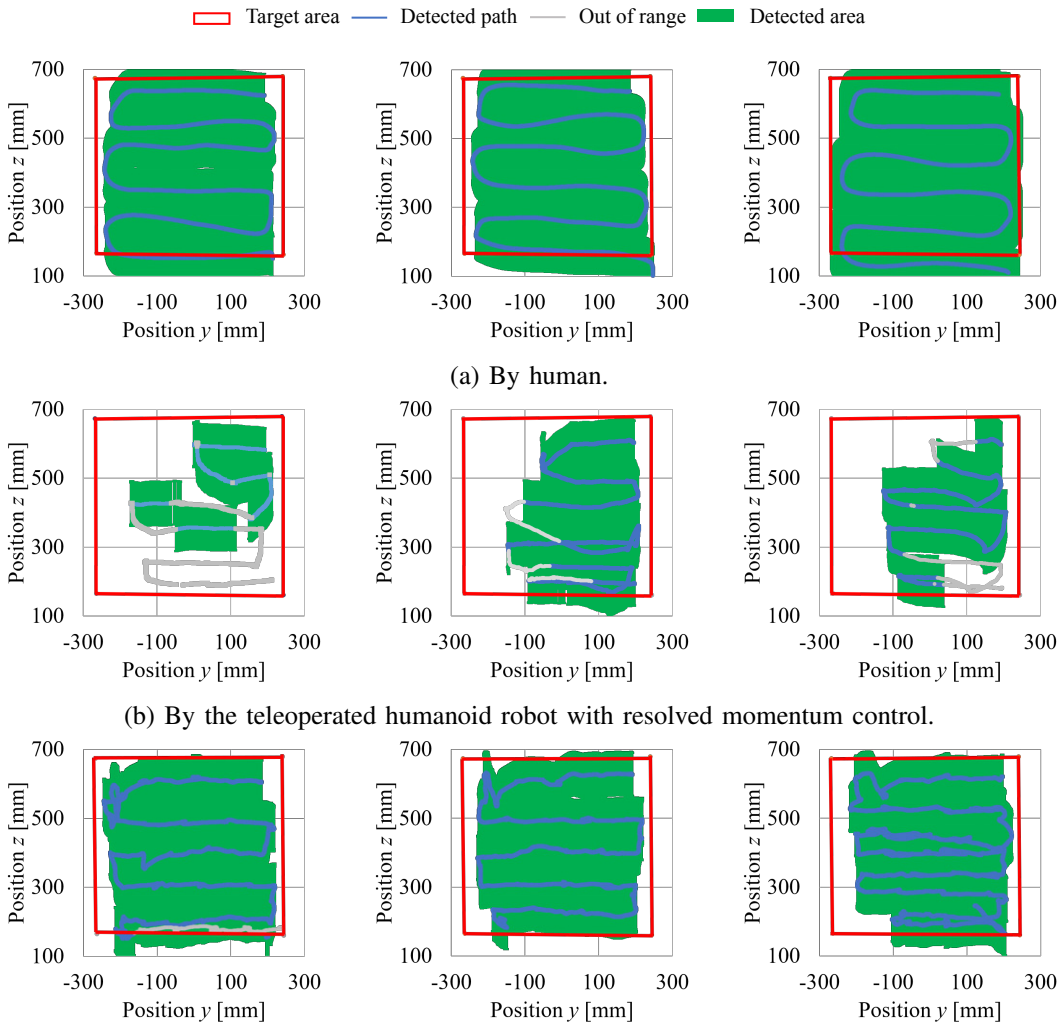

(a) By human.

(b) By the teleoperated humanoid robot with resolved momentum control.

(c) By the teleoperated humanoid robot without resolved momentum control.

Fig. 10: Comparison of scanned areas.

It was observed that the sensing range changes depending on the moving velocity of the detector. And then, remote control experiments were carried out, and the coverage areas were evaluated based on the result of the sensing range obtained by the experiment of the metal detector mentioned above. It was clarified that the coverage of the target area was not sufficient in the developed preliminary system in comparison with the case of body search by a human. In order to make the coverage larger, the developed system will be improved.

REFERENCES

[1] P. Lin, K. Abney, G. A. Bekey, "Robot Ethics: The Ethical and Social Implications of Robotics," MIT Press, Jan. 2014.

[2] H. R. Everett, D. W. Gage, "From Laboratory to Warehouse: Security Robots Meet the Real World," Int. J. of Robotics Research, July 1999, vol. 18, pp. 760–768.

[3] R. Guo, B. Li, Y. Sun, L. Han, "A Patrol Robot for Electric Power Substation," in Proc. of IEEE Int. Conf. on Mechatronics and Automation, Aug. 2009, pp. 55–59.

[4] G. Trovato, A. Lopez, R. Paredes, F. Cuellar, "Security and guidance: Two roles for a humanoid robot in an interaction experiment," in Proc. IEEE Int. Symp. on Robot and Human Interactive Communication, Aug. 2017, pp. 230–235.

[5] https://www.straitstimes.com/asia/east-asia/japans-narita-airport-to-use-security-robots-in-run-up-to-2020-olympics

[6] S. Caron, A. Kheddar, O. Tempier, "Stair Climbing Stabilization of the HRP-4 Humanoid Robot using Whole-body Admittance Control," in Proc. of IEEE Int. Conf. on Robotics and Automation, May 2019, pp. 277–283.

[7] H. Hirukawa, S. Hattori, S. Kajita, K. Harada, K. Kaneko, F. Kanehiro, M. Morisawa, S. Nakaoka, "A Pattern Generator of Humanoid Robots Walking on a Rough Terrain," in Proc. of IEEE Int. Conf. on Robotics and Automation, April 2007, pp. 2181–2187.

[8] Z. Tang and L. J. Carter, "Metal Detector Head Analysis," in Proc. Int. Conf. on Sensing Technology, Nov. 2011, pp. 93–96.

[9] http://emanual.robotis.com/docs/en/platform/thormang3/introduction/

[10] S. Kim, *et al.*, "Approach of Team SNU to the DARPA Robotics Challenge finals," in Proc. IEEE-RAS Int. Conf. on Humanoid Robots, Nov. 2015, pp. 777–784.

[11] http://www.forcedimension.com/products/omega-7/overview

[12] M. Quigley, K. Conley, B. Gerkey, J. Faust, T. Foote, J. Leibs, E. Berger, "ROS: an open-source Robot Operating System," IEEE Int. Conf. on Robotics and Automation Workshop on Open Source Robotics, May 2009.

[13] S. Kajita, F. Kanehiro, K. Kaneko, K. Fujiwara, K. Harada, K. Yokoi and H. Hirukawa, "Resolved Momentum Control: Humanoid Motion Planning based on the Linear and Angular Momentum," in Proc. IEEE/RSJ Int. Conf. on Intelligent Robots and Systems, Oct. 2003, vol. 2, pp. 1644–1650.